Journal of Sound and Vibration (2002) **252**(3), 493–507
doi:10.1006/jsvi.2001.4033, available online at http://www.idealibrary.com on IDEAL®

MODELLING AND VIBRATION CONTROL OF BEAMS WITH PARTIALLY DEBONDED ACTIVE CONSTRAINED LAYER DAMPING PATCH

D. Sun and L. Tong

School of Aerospace, Mechanical and Mechatronic Engineering, The University of Sydney, New South Wales 2006, Australia. E-mail: ltong@aeromech.usyd.edu.au

(*Received* 6 *April* 2001, *and in final form* 22 *August* 2001)

A detailed model for the beams with partially debonded active constraining damping (ACLD) treatment is presented. In this model, the transverse displacement of the constraining layer is considered to be non-identical to that of the host structure. In the perfect bonding region, the viscoelastic core is modelled to carry both peel and shear stresses, while in the debonding area, it is assumed that no peel and shear stresses be transferred between the host beam and the constraining layer. The adhesive layer between the piezoelectric sensor and the host beam is also considered in this model. In active control, the positive position feedback control is employed to control the first mode of the beam. Based on this model, the incompatibility of the transverse displacements of the active constraining layer and the host beam is investigated. The passive and active damping behaviors of the ACLD patch with different thicknesses, locations and lengths are examined. Moreover, the effects of debonding of the damping layer on both passive and active control are examined via a simulation example. The results show that the incompatibility of the transverse displacements is remarkable in the regions near the ends of the ACLD patch especially for the high order vibration modes. It is found that a thinner damping layer may lead to larger shear strain and consequently results in a larger passive and active damping. In addition to the thickness of the damping layer, its length and location are also key factors to the hybrid control. The numerical results unveil that edge debonding can lead to a reduction of both passive and active damping, and the hybrid damping may be more sensitive to the debonding of the damping layer than the passive damping.

1. INTRODUCTION

In recent years, considerable attention has been concentrated on the active constrained layer damping (ACLD) treatment in vibration control of flexible structures. The active constrained layer damping treatment was developed by combining the active control and the passive constraining layer damping (PCLD) treatment. A typical ACLD consists of a viscoelastic damping layer sandwiched between the host structure and the active constraining layer, which is made of smart materials such as piezoelectric ceramics and magnets rather than conventional materials [1–3]. The active layer can function as a conventional constraining layer to enhance the energy dissipation by enlarging the shear strain in the damping layer. On the other hand, the active layer is also used as the actuator to perform active control. Both passive and active control (i.e., hybrid control) can be performed in the ACLD treatment, and consequently, better control results can be achieved and the robustness and reliability of the closed control system can be greatly improved. Therefore, great efforts have been made on modelling, finite element method,

0022-460X/02/$35.00

control laws, experiment, stability and controllability of the ACLD-treated structures [4–16].

There are two fundamental assumptions in previous studies on ACLD. One assumption is that the transverse displacements of the constraining layer and the host structures are compatible. Under this assumption, the transverse displacements of all points on a cross-section are identical, which means that the viscoelastic layer does not undergo any peel strain. However, the studies in adhesive joints [17] show that both the shear and peel stresses in the adhesive layer may be very large in the region near an overlap end. For the sandwiched damping layer, it is indicated that the difference between the transverse displacement of the host beam and that of the constraining layer becomes significant in the regions near its ends. When the thickness of the viscoelastic core increases, the transverse displacement incompatibility will increase, particularly for the case that the beam is only partially treated by ACLD. Another assumption is that the ACLD treatment is perfectly bonded on the host structures. However, during the lifetime of the active constraining layer damping treatment, the debonding between the host and the active layer may occur due to a sudden loading or fatigue of the damping layer. As a result, the constraining layer and the host beam will vibrate separately, which may significantly alter the passive and active control of the structures. Therefore, investigation on the impact of debonding of the viscoelastic core from the host beam on passive and active control is of great importance. Up to now, few literatures were found to stress this issue.

To better understand the effects of this incompatibility of the transverse displacements and the debonding of the damping layer on the hybrid control, a model for the beam with partially debonded ACLD treatments is presented in this paper. In this model, both peel and shear strains in the viscoelastic core are considered. The debonding of the viscoelastic core from the host beam is modelled based on the assumption that no load transfers between the active constraining layer and the host in the debonded region. In active control, the positive position feedback method is employed to perform the vibration control of the beam with ACLD treatment. Based on this model, the incompatibility between the transverse displacement of the active constraining layer and that of the host beam is examined. Furthermore, the effects of the debonding of the viscoelastic core on passive and hybrid control are also investigated via a simulation example.

2. GOVERNING EQUATIONS

Consider a slender beam partially treated with ACLD and piezoelectric sensor patch, as shown in Figure 1. The piezoelectric actuator layer is also used as a constraining layer. It is assumed that the viscoelastic layer and the adhesive layer only carry constant transverse shear and peel strains. It is also assumed that there is no stress transfer between the piezoelectric constraining layer (actuator) and the host beam in the through-width-debonding region. The contact and friction in the debonded region are not considered for simplicity. In addition, only the adhesive layer used to bond the sensor patch is considered since the sensor patch is usually very thin.

The entire beam has different governing equations in its different segments. For the parts of the beam treated with ACLD and the sensor layer, its free body is shown in Figure 2 and its equations of motion can be derived as follows:

$$\rho_1 \ddot{u}_1 = T_{1,x} + b\tau_v, \qquad \rho_1 \ddot{w}_1 = Q_{1,x} + b\sigma_v, \qquad M_{1,x} + b\tau_v h_1/2 - Q_1 = 0, \quad \text{(1a–c)}$$

$$\rho_2 \ddot{u}_2 = T_{2,x} - b\tau_v + b\tau_{ad} + f_l(x, t), \quad \text{(2a)}$$

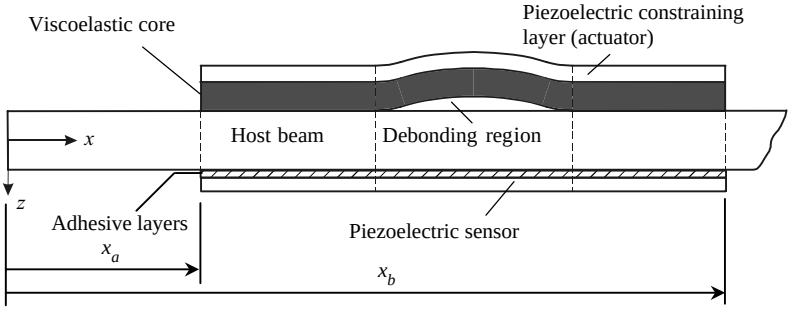

Figure 1. The composite beam with debonded ACLD treatment.

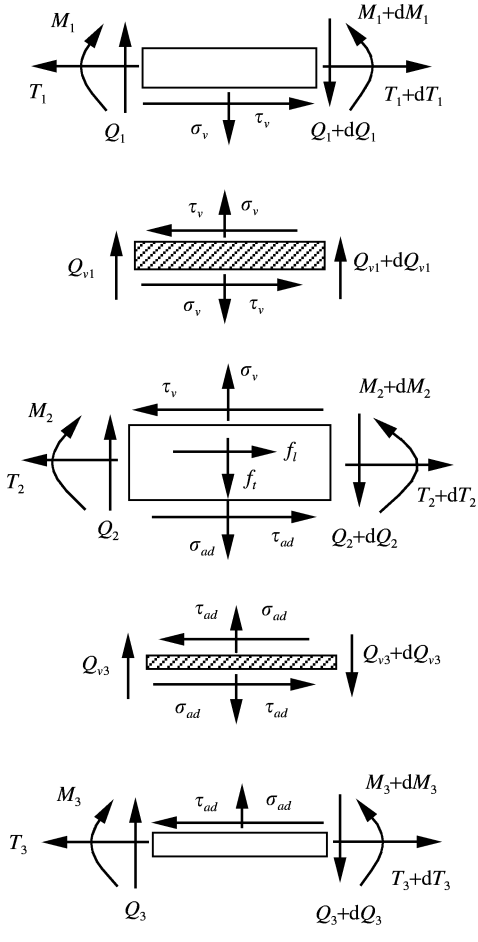

Figure 2. Free-body diagram of the beam with ACLD and piezoelectric sensor.

$$\rho_2 \ddot{w}_2 = Q_{2,x} - b\sigma_v + b\sigma_{ad} + f_t(x, t), \tag{2b}$$

$$M_{2,x} + b(\tau_v + \tau_{ad})h_2/2 - Q_2 = 0, \tag{2c}$$

$$\rho_3 \ddot{u}_3 = T_{3,x} - b\tau_{ad}, \qquad \rho_3 \ddot{w}_3 = Q_{3,x} - b\sigma_{ad}, \qquad M_{3,x} + b\tau_{ad}h_3/2 - Q_3 = 0, \tag{3a–c}$$

where the subscripts 1, 2, 3, v and ad represent the piezoelectric actuator layer, the host beam, sensor layer, the viscoelastic layer and the adhesive layer used to bond the piezoelectric sensor, respectively, u is the longitudinal displacement in mid-plane, w is the transverse displacement, h is the thickness, b is the width of the composite beam, τ and σ are the shear and the peel stress in the viscoelastic or adhesive layer, T, Q and M are the axial stress resultant, shear stress resultant and bending moment, respectively, $f_l(x, t)$ and $f_t(x, t)$ are the axial and transverse loads per unit length, and ρ is the equivalent mass densities per unit length of composite beam in which the mass of the adhesive layers and viscoelastic core is considered. The axial stress resultants and moments in Equations (1)–(3) are given by

$$T_i = A_i u_{i,x} - B_i w_{i,xx} - b e_{31i} V_i, \qquad i = 1, 2, 3, \tag{4a}$$

$$M_i = B_i u_{i,x} - D_i w_{i,xx} - b e_{31i} r_i V_i, \quad i = 1, 2, 3, \tag{4b}$$

where e_{31i} is the piezoelectric stress constant (for the host beam, $e_{312} = 0$), r_i the z-co-ordinate of the mid-plane from their own neutral planes, V_i the voltage applied on the three layers along their thickness direction (for the sensor, $V_3 = 0$), A_i and D_i the axial and bending stiffness, and B_i the extension–bending coupling term given by

$$A_i = \int_{z_{li}}^{z_{ui}} b Y_i \, \mathrm{d}z, \quad B_i = \int_{z_{li}}^{z_{ui}} b Y_i z \, \mathrm{d}z, \qquad D_i = \int_{z_{li}}^{z_{ui}} b Y_i z^2 \, \mathrm{d}z,$$

where z_{li} and z_{ui} are the z-co-ordinates of the lower and upper surfaces of the actuator layer measured from its own neutral plane.

The peel and shear stresses in the viscoelastic layer and adhesive layer can be expressed as

$$\tau_v = k_b G_v \left[\frac{1}{2h_v} (h_1 w_{1,x} + h_2 w_{2,x}) + \frac{u_2 - u_1}{h_v} \right], \tag{5a}$$

$$\sigma_v = \frac{k_b Y_v (1 - \mu_v)}{(1 - 2\mu_v)(1 + \mu_v)} \left(\frac{w_2 - w_1}{h_v} \right), \tag{5b}$$

$$\tau_{ad} = G_{ad} \left[\frac{1}{2h_{ad}} (h_2 w_{2,x} + h_3 w_{3,x}) + \frac{u_3 - u_2}{h_{ad}} \right], \tag{6a}$$

$$\sigma_{ad} = \frac{Y_{ad} (1 - \mu_{ad})}{(1 - 2\mu_{ad})(1 + \mu_{ad})} \left(\frac{w_3 - w_2}{h_{ad}} \right), \tag{6b}$$

where μ is the Poisson ratio. Note that the elastic constants of the viscoelastic core and the bonding layer along their thickness direction are modified because they are constrained by the host beam and the piezoelectric layer. Moreover, a parameter k_b has been introduced to express the bonding performance between the viscoelastic core and the host and is defined by

$$k_b = \begin{cases} 0 & \text{debonding,} \\ 1 & \text{perfect bonding.} \end{cases} \tag{7}$$

Eliminating the force and moment results in equations (1)–(6), six differential equations in terms of displacements of the composite beam can be obtained. When only electric load is considered, by introducing $\mathbf{Y}_i = (u_i, T_i, w_i, w_{i,x}, Q_i, M_i)^{\mathrm{T}}$; $i = 1, 2, 3$ as the state vector, equations (1)–(6) can be rearranged in the following state form:

$$\frac{\partial \mathbf{Y}_p}{\partial x} = \mathbf{M}_p \ddot{\mathbf{Y}}_p + \mathbf{A}_p \mathbf{Y}_p + \mathbf{B}_p V, \tag{8}$$

where $\mathbf{Y}_p = (\mathbf{Y}_1^{\mathrm{T}}, \mathbf{Y}_2^{\mathrm{T}}, \mathbf{Y}_3^{\mathrm{T}})^{\mathrm{T}}$ is the 18-dimensional state vector, $\mathbf{M}_p$ is the 18×18 mass density matrix, $\mathbf{A}_p$ is the 18×18 state matrix, and $\mathbf{B}_p$ is the 18-dimensional vector related to the control voltage on the actuator layer. Note that equation (8) is a set of complex partial differential equations when a complex modulus of the viscoelastic layer is used.

For the host beam itself, the basic equations are easily written according to the classical beam theory, which can also be written in the state equation form as

$$\frac{\partial \mathbf{Y}_2}{\partial x} = \mathbf{M}_b \ddot{\mathbf{Y}}_2 + \mathbf{A}_b \mathbf{Y}_2, \tag{9}$$

where $\mathbf{M}_b$ is the 6×6 mass density matrix and $\mathbf{A}_b$ the 6×6 state matrix of the host beam.

2.1. CONTINUITY CONDITIONS

At the interface of the perfectly bonded and debonded regions, the continuity of the displacements must be ensured. Moreover, the continuity (equilibrium) conditions of the stress resultants and moments should also be imposed to guarantee the equilibrium of the force system at the interface, as shown in Figure 3. At the interfaces between the perfectly bonded and debonded areas in the viscoelastic damping layer, the continuity conditions of displacements in the actuator layer, the host beam and the sensor layer can be expressed as

$$u_i^b = u_i^d, \qquad w_i^b = w_i^d, \qquad w_{i,x}^b = w_{i,x}^d, \quad i = 1, 2, 3, \tag{10a}$$

where the superscripts b and d represent the bonded and debonded regions respectively.

The equilibrium of the force system at the interface requires (if there is no concentrated external force is applied at the interface)

$$T_i^b = T_i^d, \qquad Q_i^b = Q_i^d, \qquad M_i^b = M_i^d, \quad i = 1, 2, 3. \tag{10b}$$

The 18 continuity equations in equations (10a) and (10b) can be rewritten in the following compact form:

$$\mathbf{Y}_p^b = \mathbf{Y}_p^d. \tag{10c}$$

In addition, all the displacements and stress resultants of the host beam at the interface between the part with ACLD treatment and part without ACLD treatment can be expressed as (Figure 3)

$$\begin{aligned} u_2^t &= u_2^n, w_2^t = w_2^n, w_{2,x}^t = w_{2,x}^n, \\ T_2^t &= T_2^n, Q_2^t = Q_2^n, M_2^t = M_2^n, \end{aligned} \tag{11a}$$

where the superscripts t and n represent the parts of the host beam with and without ACLD treatment respectively. The six continuity equations in equation (11a) can be simply expressed as

$$\mathbf{Y}_2^t = \mathbf{Y}_2^n. \tag{11b}$$

2.2. BOUNDARY CONDITIONS

The boundary conditions of the host beam, the piezoelectric actuator and sensor patches should be also imposed. In general, the boundary conditions at the ends of the piezoelectric

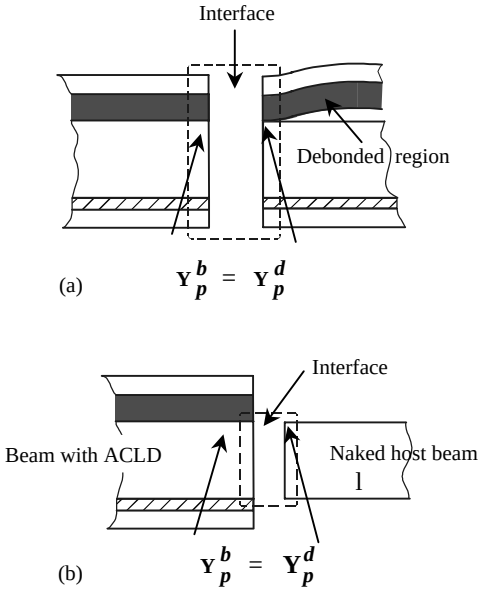

Figure 3. Continuity conditions at the interfaces: (a) interface of perfectly bonded and debonded regions, and (b) interface of ACLD treated and untreated regions.

patches and the host beam can be expressed as

$$\begin{aligned} \mathbf{R}_{1l}\mathbf{Y}_1(x_a) + \mathbf{R}_{1r}\mathbf{Y}_1(x_b) &= \mathbf{R}_1, \\ \mathbf{R}_{2l}\mathbf{Y}_2(0) + \mathbf{R}_{2r}\mathbf{Y}_2(L) &= \mathbf{R}_2, \\ \mathbf{R}_{3l}\mathbf{Y}_3(x_a) + \mathbf{R}_{3r}\mathbf{Y}_3(x_b) &= \mathbf{R}_3, \end{aligned} \tag{12}$$

where x_a and x_b are the co-ordinates of the ends of the piezoelectric patches, respectively, $\mathbf{R}_{il}$ and $\mathbf{R}_{ir}$ are the 6×6 matrices dependent on the condition at the left end and the right end, and $\mathbf{R}_i$ are the six-dimensional vectors. In this paper, the ends of the piezoelectric are free, therefore,

$$\mathbf{R}_{1l} = \mathbf{R}_{3l} = \begin{bmatrix} 0 & 1 & 0 & 0 & 0 & 0 \\ 0 & 0 & 0 & 0 & 1 & 0 \\ 0 & 0 & 0 & 0 & 0 & 1 \\ 0 & 0 & 0 & 0 & 0 & 0 \\ 0 & 0 & 0 & 0 & 0 & 0 \\ 0 & 0 & 0 & 0 & 0 & 0 \end{bmatrix}, \quad \mathbf{R}_{1r} = \mathbf{R}_{3r} = \begin{bmatrix} 0 & 0 & 0 & 0 & 0 & 0 \\ 0 & 0 & 0 & 0 & 0 & 0 \\ 0 & 0 & 0 & 0 & 0 & 0 \\ 0 & 1 & 0 & 0 & 0 & 0 \\ 0 & 0 & 0 & 0 & 1 & 0 \\ 0 & 0 & 0 & 0 & 0 & 1 \end{bmatrix}, \quad \mathbf{R}_1 = \mathbf{R}_3 = \begin{bmatrix} 0 \\ 0 \\ 0 \\ 0 \\ 0 \\ 0 \end{bmatrix}.$$

For a cantilevered host beam with a concentrated lateral force p_0 applied at its free end

$$\mathbf{R}_{2l} = \begin{bmatrix} 1 & 0 & 0 & 0 & 0 & 0 \\ 0 & 0 & 1 & 0 & 0 & 0 \\ 0 & 0 & 0 & 1 & 0 & 0 \\ 0 & 0 & 0 & 0 & 0 & 0 \\ 0 & 0 & 0 & 0 & 0 & 0 \\ 0 & 0 & 0 & 0 & 0 & 0 \end{bmatrix}, \quad \mathbf{R}_{2r} = \begin{bmatrix} 0 & 0 & 0 & 0 & 0 & 0 \\ 0 & 0 & 0 & 0 & 0 & 0 \\ 0 & 0 & 0 & 0 & 0 & 0 \\ 0 & 1 & 0 & 0 & 0 & 0 \\ 0 & 0 & 0 & 0 & 1 & 0 \\ 0 & 0 & 0 & 0 & 0 & 1 \end{bmatrix}, \quad \mathbf{R}_2 = \begin{bmatrix} 0 \\ 0 \\ 0 \\ 0 \\ p_0 \\ 0 \end{bmatrix}$$

in which $Q_2 = p_0$ is included at the free end of the host beam.

2.3. SENSOR EQUATION

To perform active control of the beam, the vibration signal must be sensed by the piezoelectric layer. The charge accumulated on the electrodes of the piezoelectric sensor layer can be evaluated as

$$q(t) = \int_{L_s} be_{313} \frac{\partial u_3}{\partial x} \, \mathrm{d}x - \int_{L_s} be_{313} r_3 \frac{\partial^2 w_3}{\partial x^2} \, \mathrm{d}x, \tag{13}$$

where L_s is the integration interval related to the sensor layer. The charge signal measured by the sensor can be used to perform the active control of the beam.

2.4. CONTROL LAW

Due to the presence of the longitudinal vibration and the incompatibility of the transverse displacements of the actuator and host beam, the widely used direct feedback control method cannot guarantee the stability of the closed-loop system [18]. Therefore, the positive position feedback method [19] is employed to control the first mode of the beam. In this method, the control voltage is designed by

$$V(t) = g\eta(t), \tag{14}$$

where $g \geqslant 0$ is a control gain, and $\eta(t)$ is the output of a compensator given by

$$\ddot{\eta}(t) + 2\zeta_c \omega_c \dot{\eta}(t) + \omega_c^2 \eta(t) = \omega_c^2 q(t) \tag{15}$$

where ω_c and ζ_c are the natural frequency and damping ratio of the compensator respectively. When the first mode is chosen as the target mode, ω_c is taken as the first frequency of the composite beam. In this case, the compensator in equation (15) functions as a low-pass filter and a phase shifter, and its output $\eta(t)$ is proportional to the first modal velocity of the composite beam. As a result, an active damping can be achieved by the control law in equation (14). Since only the charge output of the sensor is needed to design the control voltage, the control can be easily implemented in practice.

3. SOLUTION SCHEME

When the host beam is partially treated by the ACLD, especially when the debonding is introduced, its governing equations have different forms in different segments. To solve such a set of partial differential equations, the Fourier transformation method is employed.

Taking Fourier transformation on both sides of equation (8), we have

$$\frac{\mathrm{d}\bar{\mathbf{Y}}_p}{\mathrm{d}x} = (\mathbf{A}_p - \omega^2 \mathbf{M}_p)\bar{\mathbf{Y}}_p + \mathbf{B}_p \bar{V}, \tag{16}$$

where ω is the frequency parameter, the overbar stands for the Fourier transformation, for example,

$$\bar{\mathbf{Y}}_p(x, \omega) = \int_{-\infty}^{\infty} \mathbf{Y}_p(x, t) \mathrm{e}^{-\mathrm{j}\omega t} \, \mathrm{d}t,$$

where $j = \sqrt{-1}$. Taking Fourier transformation in equations (14) and (15) gives

$$\bar{V}(\omega) = gG(\omega)\bar{q}(\omega), \tag{17}$$

where $G(\omega) = 1/(1 - \lambda^2 + 2\zeta_c\lambda j)$ is the transfer function of the compensator, in which $\lambda = \omega/\omega_c$. Substituting equation (17) into equation (16), the closed-loop equations of the segment treated with ACLD in the frequency domain can be obtained as

$$\frac{d\bar{\mathbf{Y}}_p}{dx} = (\mathbf{A}_p - \omega^2\mathbf{M}_p)\bar{\mathbf{Y}}_p + gG(\omega)\bar{q}(\omega)\mathbf{B}_p. \tag{18}$$

Similarly, after taking Fourier transformation, the governing equations of the host beam in equation (9) becomes

$$\frac{d\mathbf{Y}_2}{dx} = (\mathbf{A}_b - \omega^2\mathbf{M}_b)\mathbf{Y}_2. \tag{19}$$

The complex governing equations together with their related boundary conditions form a complicated boundary value problem. The multiple shooting method [20] is generalized to solve this problem and numerical results in the frequency domain have been obtained. Once the boundary problem is numerically solved in the frequency domain, its solution in the time domain can be obtained by taking inverse Fourier transformation.

4. NUMERICAL EXAMPLE

As an example, consider a cantilever beam treated with ACLD patch, which is clamped at its left end as shown in Figure 4. The properties and dimensions are given in Table 1. The free vibration of the beam is excited by an initial transverse impulse of 0·1 N s acted at its free end. The effects of the thickness, location and length of the viscoelastic damping layer on the hybrid control will be investigated. Furthermore, the effects of the debonding of the viscoelastic damping layer are also examined in this section.

First, we evaluate the difference between the transverse displacement of the active constraining layer and that of the host beam. To this end, a 4 cm long ACLD patch is bonded on the host beam and its left end is 2 cm away from the clamped end of the host beam. For the open-loop system, the transverse displacements w_1 and w_2 at the right end of the ACLD patch are calculated for the first five modes. The relative differences of their amplitude $|(w_1 - w_2)/w_2|$ and that of their phase angle $|[\arg(w_1) - \arg(w_2)]/\arg(w_2)|$ are presented in Figures 5(a)–5(d), respectively, for different thicknesses of the damping layer. For the closed-loop system, the first mode is controlled by taking $g = 2 \times 10^8$ and $\zeta_c = 0.5$ in equations (14) and (15), and the relative amplitude and phase differences are also given in

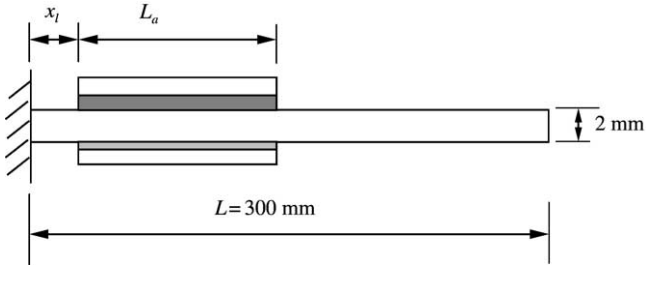

Figure 4. A cantilevered beam with ACLD patch.

TABLE 1

Physical properties and dimensions of the ACLD beam

Item	Host beam (steel)	Actuator (PZT-5A)	Viscoelastic core	Sensor (PZT-5A)	Adhesive layer
Mass density (kg/m^3)	7800	7600	1600	7600	1600
Y(GPA)	210	63	$0{\cdot}01(1 + 1{\cdot}05i)$	63	2·4
The Poisson ratio			0·4		0·34
e_{31} (N/Vm)	—	23·31	—	23·31	—
Thickness (m)	0·002	0.001		0.0004	0·00015
Length (m)	0·3				
Width (m)	0·02	0·02	0·02	0·02	0·02

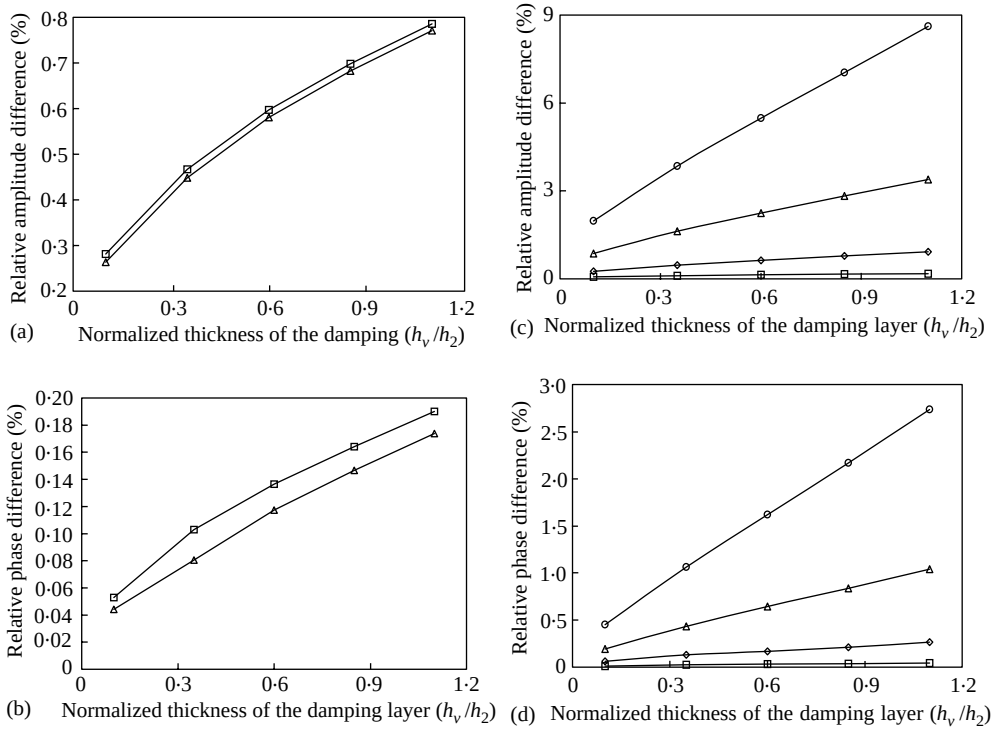

Figure 5. Relative difference of the transverse displacements at the right end of the ACLD patch: (a) amplitude difference $|(w_1 - w_2)/w_2|$ for mode 1, (b) phase difference $|[\arg(w_1) - \arg(w_2)]/\arg(w_2)|$ for mode 1, (c) amplitude difference $|(w_1 - w_2)/w_2|$ for modes 2–5 (open loop), and (d) phase difference $|[\arg(w_1) - \arg(w_2)]/\arg(w_2)|$ for modes 2–5 (open loop). —□—, Open loop; —△—, closed loop. —□—, Mode 2; —◇—, mode 3; —△—, mode 4; —○—, mode 5.

Figures 5(a) and 5(b) respectively. Figure 5 shows that both the amplitudes and phase angles of the transverse displacements in the active constraining layer and host beam are different. Moreover, these differences increase remarkably as the thickness of the damping layer increases. However, this trend is hardly affected by the closed-loop control although the active control may slightly decrease the amplitude and phase differences between w_1 and w_2. It can also be found that the amplitude and phase differences between w_1 and w_2 become more significant for higher modes of the beam. For example, when the damping layer is 1·1 times as thick as the host beam, these amplitude and phase differences at the fifth mode are

nearly 9 and 3%, respectively, while those at the first mode are only 0·8 and 0·2%. It should be pointed that the phase incompatibility of the transverse displacement in actuator and sensor bonded on the host beam may result in instability in the closed-loop control. The difference between the transverse displacement of the constraining layer and the host beam along the ACLD span can be determined from the peel strain distribution in the damping layer shown in Figure 6. Figure 6 depicts the distribution of the peel and shear strains in the viscoelastic damping layer with different thicknesses for the first three modes of the open-loop system. It shows that both peel and shear strains in the regions near the ends of the damping layer are much larger than those in the middle region. Moreover, the strain distribution for all modes depends on the thickness of the damping layer. For all the three modes, as indicated in Figures 6(b), 6(d) and 6(f), the shear strain decreases remarkably as the thickness of damping layer increases. However, as shown in Figures 6(a), 6(c) and 6(e), the relationship between the peel strain and the thickness of damping layer is not so simple particularly for the higher modes. This is probably because the incompatibility of transverse vibration between the host and the actuator layer affects the peel strain much more than the shear strain. Figure 6 also shows that the incompatibility of the transverse displacement is more severe in the regions near the ends of the ACLD patch for a damping layer with a given thickness.

Next, we mainly examine the passive and hybrid (active plus passive) damping effects of the ACLD patch on the first mode of the composite beam. When the ACLD patch mentioned above was used to perform the passive and active control, the damping ratios for

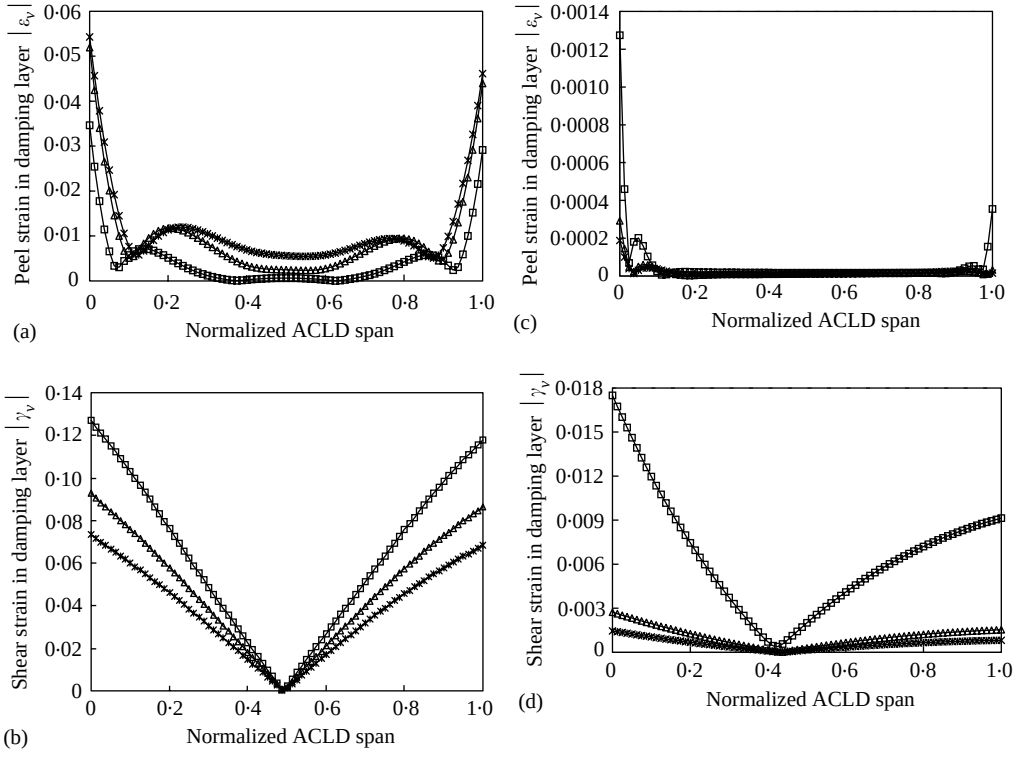

Figure 6. The modal strain distribution in the damping layer: (a) peel strain for mode 1, (b) shear strain for mode 1, (c) peel strain for mode 2, (d) shear strain for mode 2, (e) peel strain for mode 3, and (f) shear strain for mode 3. (a–e) —□—, $h_v/h_2 = 0{\cdot}1$; —△—, $h_v/h_2 = 0{\cdot}6$; —★— $h_v/h_2 = 1{\cdot}1$. —□—, $h_v/h_a = 0{\cdot}1$; —△—, $h_v/h_a = 0{\cdot}6$; —★—, $h_v/h_a = 1.1$.

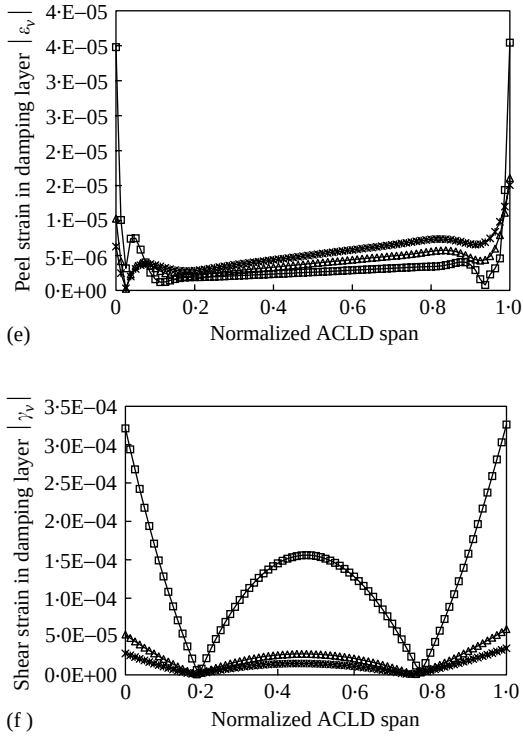

Figure 6. Continued.

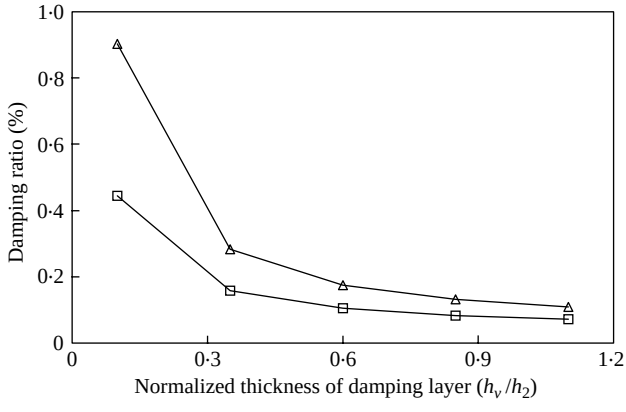

Figure 7. Effect of the thickness of the damping layer on the damping ratio for the first mode: —□—, open loop; —△—, closed loop.

the first mode of the beam are as displayed in Figure 7. As indicated in Figure 7, both passive and hybrid damping effects on the first mode of the beam are greatly weakened with an increasing thickness of the damping layer. The reduction of the passive damping results from the decrease of the shear strain due to the thickening of the damping layer, as shown in Figure 6. The incompatibility between the transverse displacements on the actuator and the host beam may be one of the factors affecting the efficiency of the hybrid control. Figure 8

presents the effect of the location of a 4 cm ACLD patch (the thickness of the damping layer is 2 mm) on passive and hybrid control of the first mode. In Figure 8, x_l represents the x-co-ordinate of the left end of the ACLD patch, and L is the length of the host beam. Figure 8 shows that the best location of the ACLD patch for both passive and hybrid control of the first mode is near the clamped end of beam. The length of the ACLD is also a key factor to affect the passive and active control, as shown in Figure 9. In this case, the distance from the clamped end of the beam to the left end of the ACLD patch remains as 1 cm. The lengths of the ACLD patch are normalized by the whole length of the beam. Figure 9 indicates that both the passive and hybrid damping ratios for the first mode are enlarged when the ACLD patch increases. The hybrid damping is much more sensitive to the length change of ACLD patch than the passive damping.

Finally, we investigate how the edge and middle debonding of the damping layer affects the passive and hybrid control of the composite beam. An 8 cm ACLD patch with 2 mm thick damping layer is bonded on the beam such that its left end is 1 cm away from the clamped end of the beam. The edge debonding regions with several different lengths are located at the left end of the ACLD patch. When a 50% edge debonding occurs, the frequency spectrum of the transverse displacement at the free end of the open-loop beam is

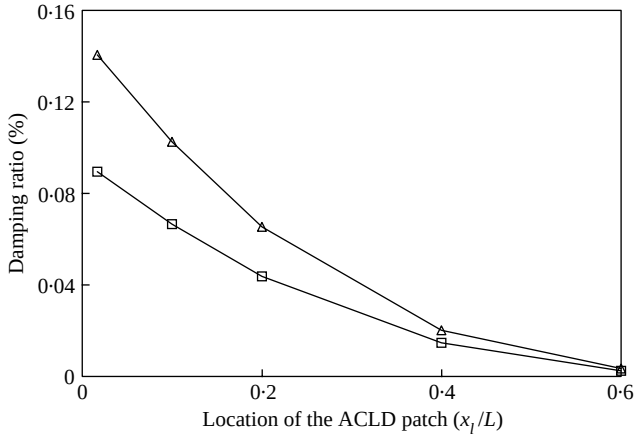

Figure 8. Effect of the location of the ACLD patch on the damping ratio for the first mode: —□—, open loop; —△—, closed loop.

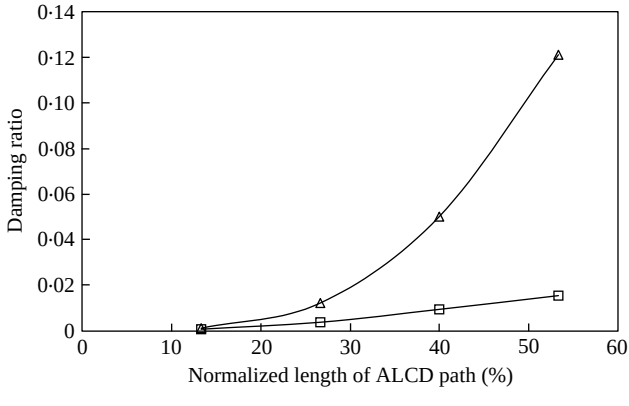

Figure 9. Effect of the length of the ACLD patch on the damping ratio for the first mode: —□—, open loop; —△—, closed loop.

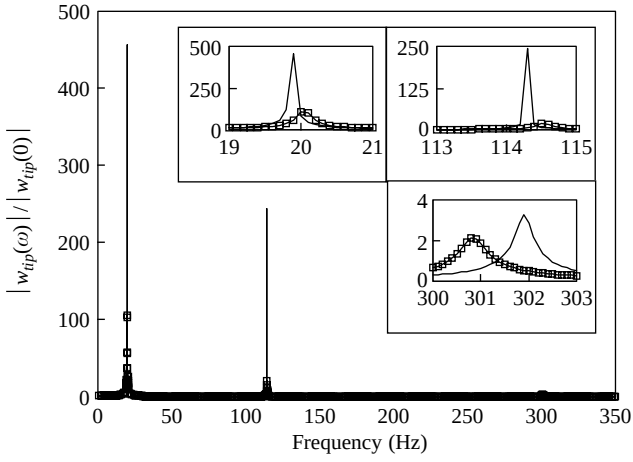

Figure 10. Frequency spectrum of the transverse displaceent at the free and (open loop): —□—, perfect bonding; ——, 50% edge debonding.

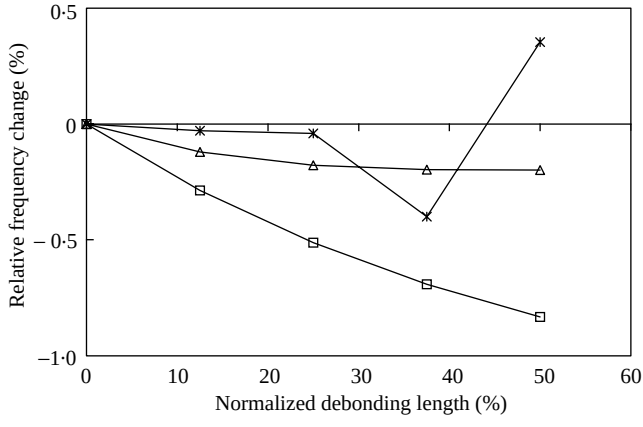

Figure 11. Debonding of damping layer on frequencies of the beam: —□—, mode 1; —△—, mode 2; —★—, mode 3.

given in Figure 10. For the purpose of comparison, the frequency spectrum for the beam with perfect bonded ACLD is also shown in Figure 10. It can be seen from Figure 10 that the edge debonding of the ACLD results in a significant change in the frequency spectrum. The peak values in the spectrum increase due to the decreased damping caused by the edge debonding. Moreover, the modal frequencies are also changed to some extent due to the debonding, which leads to the change of the locations of the peaks in the frequency spectrum. To further examine the effects of edge debonding on frequencies and damping ratios of the beam, take the edge debonding length as 0, 12·5, 25, 37·5 and 50% of the total length of the damping layer, respectively, the relative change of the first three modal frequencies are depicted in Figure 11. The edge debonding of the ACLD from the host beam leads to reduction of the first two modal frequencies, and the first two frequencies decrease as the edge debonding length becomes larger. However, when the edge debonding length reaches half of the entire length of the damping layer, the third frequency is higher than that with perfectly bonded ACLD. It is believed that, because the first frequency of the debonded constraining layer, which vibrates in a way similar to a cantilever beam, is about 291 Hz and

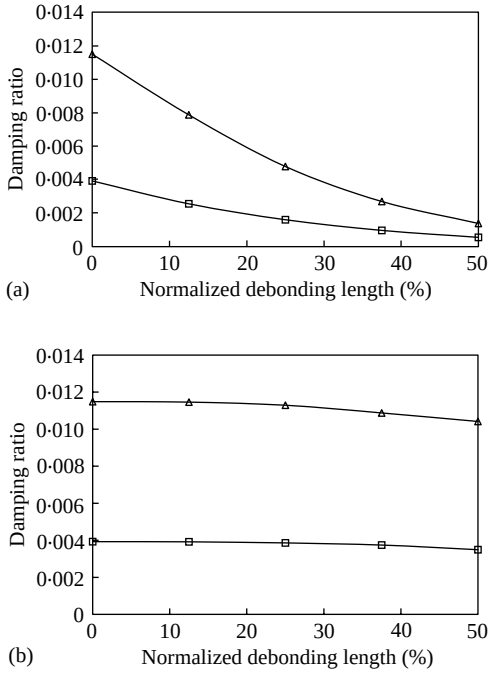

Figure 12. Effect of debonding of the damping layer on the damping ratios for mode 1: (a) edge debonding and (b) middle debonding. —□—, open loop; —△—, closed loop.

is close to the third frequency of the beam (300 Hz), the two vibration modes interact with each other. The impact of the edge debonding of ACLD on passive and hybrid vibration control of the beam is presented in Figure 12(a). Both passive and hybrid damping effects are significantly reduced due to the edge debonding of the viscoelastic damping layer. The longer the edge debonding region is, the more significant the reduction of the damping ratio is. For example, a 12.5% edge debonding of the ACLD leads to a 31% reduction of the hybrid damping ratio for the first mode. However, when the debonding occurs in the middle of the damping layer, its effect on both passive and hybrid damping is very weak, as shown in Figures 12(b). Even a 50% middle debonding of the damping layer can only result in a 9% reduction of the hybrid damping ratio for mode 1. It can also be seen from both Figure 12(a) and 12(b) that the hybrid control is much more sensitive to the debonding of the damping layer than the passive control itself.

5. CONCLUSIONS

A detailed model for the beams with partially debonded ACLD treatment is presented, in which both flexural and longitudinal displacements are also taken into account. The hybrid control is performed by using the positive position feedback control to control the first mode of the beam. The simulation results show that the incompatibility of the transverse displacements is remarkable in the regions near the ends of the ACLD patch especially for the thick viscoelastic damping layer, and this incompatibility gets more significant for the higher modes. The results also show that a thinner damping layer may lead to larger passive and hybrid damping because the shear strain decreases remarkably as the thickness of the damping layer increases. Moreover, the length and location of the ACLD patch are key

factors to the hybrid control. As to the effects of the debonding, the edge debonding can lead to reduction of both passive and active damping. It is also found that the hybrid damping is more sensitive to the debonding of the damping layer than the passive damping only.

ACKNOWLEDGMENTS

The authors are grateful to the support of the National Natural Science Foundation of China (Grant No. 19802016) and the Australian Research Council through a Large Grant (Grant No. A10009074).

REFERENCES

1. A. BAZ and J. RO 1994 *Journal of Sound and Vibration* **28**, 18–21. The concept and performance of active constrained layer damping treatments.
2. I. Y. SHEN 1994 *Journal of Vibration and Acoustics* **116**, 341–349. Hybrid damping through intelligent constrained treatments.
3. M. RUZZENE, J. OH and A. BAZ 2000 *Journal of Sound and Vibration* **236**, 657–682. Finite element modelling of magnetic constrained layer damping.
4. R. K. KAPADIA and G. KAWIECKI 1997 *Journal of Intelligent Material Systems and Structures* **8**, 103–111. Experimental evaluation of segmented active constrained layer damping treatments.
5. S. C. HUANG, D. J. INMAN and E. M. AUSTIN 1996 *Smart Materials and Structures* **5**, 301–313. Some design considerations for active and passive constrained layer damping treatments.
6. J. J. HOLLKAMP and R. W. GORDON 1996 *Smart Materials and Structures* **5**, 715–722. An experimental comparison of piezoelectric and constrained layer damping.
7. D. E. VELEY and S. S. RAO 1996 *Smart Materials and Structures* **5**, 660–671. A comparison of active, passive and hybrid damping in structural design.
8. S. POH, A. BAZ and B. BALACHANDRAN 1996 *Smart Materials and Structures* **5**, 649–659. Experimental adaptive control of sound radiation from a panel into an acoustic cavity using active constrained layer damping.
9. I. Y. SHEN 1996 *Journal of Vibration and Acoustics* **118**, 70–77. Stability and controllability of Euler–Bernoulli beams with intelligent constrained layer treatments.
10. J. A. RONGONG, J. R. WRIGHT, R. J. WYNNE and G. R. TOMLINSON 1997 *Journal of Vibration and Acoustics* **119**, 120–130. Modelling of a hybrid constrained layer/piezoceramic approach to active damping.
11. A. BAZ 1997 *Journal of Vibration and Acoustics* **119**, 166–172. Boundary control of beams using active constrained layer damping.
12. R. K. KAPADIA and G. KAWIECKI 1997 *Journal of Intelligent Material Systems and Structures* **8**, 103–111. Experimental evaluation of segmented active constrained layer damping treatments.
13. S. W. KUNG and R. SINGH 1998 *Journal of Sound and Vibration* **212**, 781–805. Vibration analysis of beams with multiple constrained layer damping patches.
14. Q. LIU, A. CHATTOPADHYAY, H. Z. GU and X. ZHOU 2000 *Smart Materials and Structures* **9**, 523–532. Use of segmented constrained layer damping treatment for improved helicopter aeromechanical stability.
15. W. H. LIAO and K. W. WANG 1998 *Journal of Vibration and Acoustics* **120**, 886–893. Characteristics of enhanced active constrained layer damping treatments with edge elements. Part 1: finite element model development and validation.
16. D. C. SUN and L. TONG 2000 in *Advances in Computational Engineering & Science* S. N. Atluri and F. W. Brust editors, Palmdale, U.S.A.: Tech Science Press. Vol. II, 1530–1535. Modeling of beams with active constrained layer damping.
17. L. TONG and G. P. STEVEN 1999 *Analysis and Design of Structural Bonded Joints*. Boston: Kluwer Academic Publishers.
18. S. Y. YANG and W. H. HUANG 1998 *Journal of Sound and Vibration* **216**, 529–538. Is a collocated piezoelectric sensor/actuator pair feasible for an intelligent beam?
19. J. L. FANSON and T. K. CAUGHEY 1990 *American Institute of Aeronautics and Astronautics Journal* **28**, 717–724. Positive position feedback control for large space structures.
20. J. STOER and R. BULIRSCH 1980 *Introduction to Numerical Analysis*, pp. 483–519. New York: Springer-Verlag.